

# XAI and Android Malware Models

Maithili Kulkarni\* Mark Stamp\*<sup>†</sup>

November 27, 2024

## Abstract

Android malware detection based on machine learning (ML) and deep learning (DL) models is widely used for mobile device security. Such models offer benefits in terms of detection accuracy and efficiency, but it is often difficult to understand how such learning models make decisions. As a result, these popular malware detection strategies are generally treated as black boxes, which can result in a lack of trust in the decisions made, as well as making adversarial attacks more difficult to detect. The field of eXplainable Artificial Intelligence (XAI) attempts to shed light on such black box models. In this paper, we apply XAI techniques to ML and DL models that have been trained on a challenging Android malware classification problem. Specifically, the classic ML models considered are Support Vector Machines (SVM), Random Forest, and  $k$ -Nearest Neighbors ( $k$ -NN), while the DL models we consider are Multi-Layer Perceptrons (MLP) and Convolutional Neural Networks (CNN). The state-of-the-art XAI techniques that we apply to these trained models are Local Interpretable Model-agnostic Explanations (LIME), Shapley Additive exPlanations (SHAP), PDP plots, ELI5, and Class Activation Mapping (CAM). We obtain global and local explanation results, and we discuss the utility of XAI techniques in this problem domain. We also provide a literature review of XAI work related to Android malware.

## 1 Introduction

Malicious software, or malware, can appear in various forms, including worms, viruses, adware, and ransomware. In recent years, the popularity of smartphones has made them targets of malware attacks.

It is not surprising that machine learning (ML) and deep learning (DL) have become dominant approaches for detecting malware, including malware on mobile devices [34]. Such models can be trained on a variety of static and dynamic features [3, 29]. We elaborate on some of these techniques in Section 2.

---

\*Department of Computer Science, San Jose State University

<sup>†</sup>mark.stamp@sjsu.edu

Although ML and DL provide significant capabilities, such techniques are generally treated as black boxes [7]. This black box aspect can limit the trust that users are willing to place in such models. Also, from a security perspective, black box models may be more susceptible to adversarial attacks, where an attacker attempts to modify a model to yield incorrect results. Furthermore, when an opaque model fails, it is difficult to identify why the model is failing. Thus, there is a need to develop insights into the internal operations of learning models, especially those that are used for malware detection and classification.

The emerging field of eXplainable Artificial Intelligence (XAI) deals with understanding the inner workings of learning models [27]. XAI generally attempts to explain model outcomes in terms of the influence of input variable (i.e., features), or by using approximation or surrogate models whose outcomes are more explainable. The goal is to provide a transparent and interpretable view of a model’s decision-making process. In this paper, we focus on XAI in the context of Android malware detection.

We consider XAI for selected classic ML techniques and DL models that have been trained on the well-known KronoDroid Android malware dataset. Specifically, the classic ML models that we consider are Support Vector Machines (SVM),  $k$ -Nearest Neighbors ( $k$ -NN), and Random Forest. In the DL realm, we consider Multi-Layer Perceptron (MLP) and Convolutional Neural Network (CNN) architectures. In general, classic ML techniques are relatively interpretable, as ML models are typically based on probabilistic, algebraic, or geometric intuition. In contrast, most neural networking models are opaque, in the sense that it is non-trivial to understand how they are making decisions. In this paper, we aim to provide a comparative study of XAI for the selected ML and DL models, within the context of Android malware classification.

For each trained model, we apply relevant XAI techniques from among the following: Local Interpretable Model-Agnostic Explanations (LIME), SHapley Additive exPlanations (SHAP), PDP, and ELI5 [18, 26, 38]. Additionally, we provide a review of recent literature where XAI techniques are applied to models trained on Android malware. Our literature review can be viewed as an extension of that in [19].

The remainder of this paper is organized as follows. Section 2 covers a range of relevant background topics, including malware detection strategies and an introduction to the XAI techniques that we employ in our experiments. Section 3 gives an overview of related previous work on malware classification and provides a literature review of recent XAI work related to models trained on Android malware. Section 4 covers the implementation of the various classic ML and DL models used in this paper, along with our experiments and results. Finally, Section 5 summarizes our work, and we provide a discussion of potential avenues for future work.

## 2 Background

In this section, we first give a brief overview of malware, followed by a discussion of ML and DL algorithms that are commonly used to classify malware. This section also includes detailed background on the state-of-the-art XAI techniques that we consider in this paper.

### 2.1 Malware and Categories

Malware is the dominant security threat to smartphones [22]. The purpose of writing malware can range from simply a prank to an organized criminal activity, information warfare, and espionage. Figure 1 highlights the rapid increase in the volume of Android malware samples over the years 2012 through 2018 [6].

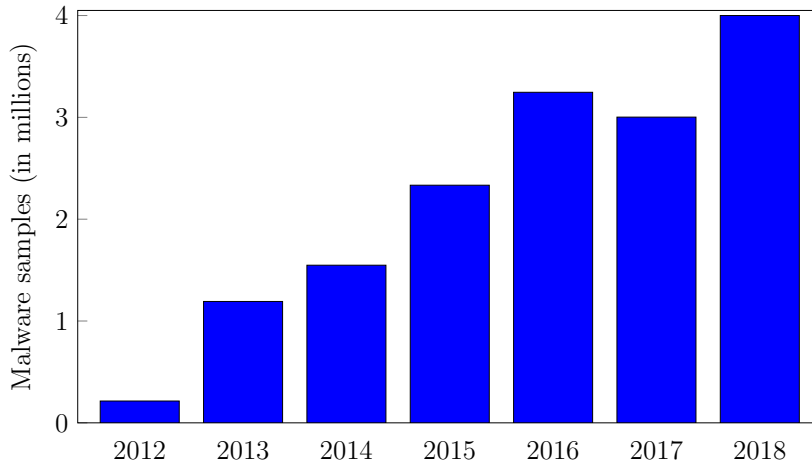


Figure 1: Detected Android malware samples

Malware covers an array of threats, including backdoors, spyware and adware, Trojan horses, and viruses. We now give a brief overview of these common types of malware before moving on to discuss malware detection techniques.

A backdoor, also known as a trapdoor, is built to circumvent security checks [22]. Programmers may create backdoors for legitimate reasons when developing their code. Cybercriminals seek to exploit their backdoors to delete files, access sensitive data, install additional malware, open communication ports for remote access, and so on.

As the name implies, spyware is used to spy on user activities, and can include recording the audio of calls on a smartphone, tracking Internet usage, recording keystrokes (including passwords), and so on [22]. Adware, on the other hand, often generates fake error messages and then asks the user to pay money to fix a non-existent problem. Winwebsec is a well-known family of adware [25].

Named after the ancient historic plot by Greek invaders to capture Troy, a Trojan is a program devised to look harmless, but secretly performs a malicious

task. Trojan apps that send premium SMS messages in the background are a typical example [22]. Zeus (aka Zbot) is a well-known Trojan family, and it has been widely used for nearly two decades for crimes including bank fraud and money laundering [13].

A virus is the most common type of malware. True to its name, this malware replicates by infecting executable programs. The infected programs can further propagate the virus during their execution, or a virus might propagate through external devices, software, or email. Like a biological virus, a computer virus might exhibit metamorphism, in the sense of changing its form when infecting other systems [33]. Metamorphism is an effective means of evading classic virus detection techniques, such as signature scanning.

## 2.2 Learning Models for Malware Detection

There is a constant arms race between malware writers and antivirus developers. Over the past two decades, ML and DL techniques have come to the fore in the fields of malware detection, classification, and analysis. In this section, we introduce the ML and DL techniques that we consider in this paper, where the underlying problem is to classify Android malware samples.

### 2.2.1 Classic Machine Learning

Support Vector Machines (SVM) [34] are popular supervised machine learning models. SVMs attempt to separate classes using hyperplanes. A nonlinear kernel can be used to map training data into a higher-dimensional space and thereby enhance the separability.

In machine learning, a Random Forest consists of an ensemble of decision trees, with voting among the component trees used to determine the classification [12]. More trees can mean better accuracy and generalizability, but care must be taken not to overfit the data.

As the name suggests, in  $k$ -Nearest Neighbors ( $k$ -NN), samples are classified based on the  $k$  nearest samples in the training set. There is no explicit training required for  $k$ -NN, and hence the algorithm is often referred to as a “lazy learner”. However, scoring calculation can be relatively expensive. The technique is highly sensitive to local structure and, in particular, for small values of  $k$ , overfitting is common [34].

### 2.2.2 Deep Learning

Artificial Neural Networks (ANNs) are mathematical models that are inspired by neurons in the brain. Multi-layer Perceptrons (MLP) are the simplest useful neural networking architecture, and hence they are sometimes referred to simply as ANNs. MLPs are feed-forward networks that generalize basic perceptrons to allow for nonlinear decision boundaries. This is analogous to the way that

nonlinear SVMs generalizes linear SVMs. As with most DL architectures, MLPs are trained using backpropagation [34].

Convolutional Neural Networks (CNNs) are a specialized type of neural network that focus on local structure, making them ideal for image analysis. CNNs are composed of an input layer, convolution layers, and pooling layers, along with a fully-connected output layer (or layers) that produce a vector of class scores. The first convolutional layer in a CNN extracts various intuitive features from the input. Subsequent convolutional layers extract ever more abstract features from the previous layer.

## 2.3 Overview of Explainable AI

The applications of artificial intelligence in the security domain introduces several challenges. For example, adversarial attacks on such systems are a concern. By employing eXplainable Artificial Intelligence (XAI) techniques to understand how a model works, we have a better chance of detecting such attacks. Additionally, XAI analysis, may enable us to perform feature reduction, based on feature importance, which can speed up detection. XAI can shed light on black box models by uncovering relationships between dependent and independent variables, thereby increasing user trust, which is especially important in security-related applications.

Next, we briefly consider XAI techniques from various perspectives. Specifically, we discuss interpretability and explanations from the perspectives of ante-hoc versus post-hoc, model-agnostic versus model-specific, and local versus global. We then consider the level of interpretability—high, medium, or low—provided by XAI techniques

Models that are inherently easy to understand are said to be ante-hoc interpretable. For example, linear models and classic Hidden Markov Models (HMM) fall into the ante-hoc interpretable category. A model is post-hoc model interpretable if we need to apply explicit interpretation methods after the model is trained. Of course, post-hoc techniques can also be used on intrinsically interpretable models after they are trained [38].

Some XAI techniques are model agnostic, in the sense that they can be applied to any type of machine learning algorithm. On the other hand, some XAI techniques are model-specific. Of the XAI techniques that we consider, LIME, SHAP, PDP plots, and ELI5 are all model-agnostic techniques, while CAM is specific to CNNs. According to [27], model-specific techniques may, in general, be more informative than model-agnostic explanation techniques.

Local interpretable techniques help us understand how and why the model makes a certain classification for a specific sample, or for a group of samples [24]. Locally, models can often be viewed as linear or monotonic in some features. Global techniques deal with interpreting a model as a whole, taking a holistic view of features into account. For example, LIME only deals with local interpretability, while SHAP can be used for both local and global explanations.

Models consisting of linear functions are highly interpretable. For example, linear SVM models are highly interpretable. For this reason, some XAI techniques, such as LIME, use linear functions as local approximations.

Models with nonlinear monotonic functions are in the class of medium interpretable models. Nonlinear functions are those in which input data is modeled using a function with a nonlinear combination of the model parameters. For example, an SVM trained with the (nonlinear) RBF kernel is a medium interpretable model.

Machine learning models with nonlinear and non-monotonic functions fall into the low interpretability category. Most DL models are in this category, and hence they are inherently difficult to interpret. CAM is model-specific technique that is applicable to CNNs, which are in the low interpretability category.

It has been suggested that there may be an inverse correlation between model performance and inherent interpretability [9, 10]. However, there are XAI techniques that are useful for models in the low interpretability category; for example, CAM is useful for interpreting CNN models, as mentioned above.

## 2.4 XAI Techniques

Before moving on to discuss our experiments, we first introduce the explainability techniques that we consider. We use feature ranking to analyze our linear SVM and Random Forest models, and for other models, we use the XAI techniques of LIME, ELI5, CAM, and SHAP (including PDP plots).

### 2.4.1 SVM and Random Forest Interpretations

Linear SVMs are inherently interpretable models, in the sense that we can determine the relative importance of features based on the model weights, assuming that the features have been properly normalized. In the `sklearn` Python library, it is easy to obtain feature weights for the linear SVM kernel using the `coef_method` [31]. Similarly, we can obtain feature rankings from Random Forest models. Non-linear SVMs, as well as the other ML and DL techniques that we consider, are not highly interpretable.

### 2.4.2 LIME

Local Interpretable Model-agnostic Explanations (LIME) is based on local surrogate interpretable models, and is used to explain individual predictions of black box machine learning models [17]. LIME generates a new dataset consisting of perturbed samples and the corresponding predictions of the black box model. Based on this new dataset, LIME then trains a simple interpretable model which is weighted by the proximity of the perturbed instances to the sample of interest. This interpretable model provides a good local approximation to the original machine learning model.

According to [30], the explanation provided by LIME of sample  $x$ , denoted  $E(x)$ , can be expressed as

$$E(x) = \operatorname{argmin}_{g \in G} (L(M, g, \pi_x) + \Omega(g))$$

where  $L$  measures the inaccuracy introduced by approximating the original model  $M$  with the simplified model  $g$  in a perturbed neighborhood defined by  $\pi_x$ . By default,  $g$  is a sparse linear model, but decision trees can also be used. Here,  $\Omega(g)$  is a measure of model complexity and acts as a penalty term, since we want a simple approximation. Note that the minimum is over the family  $G$  of possible explanations.

Obtaining LIME explanations consists of the following steps.

1. Choose a dataset.
2. Train a black box model on the dataset.
3. Generate new data samples by perturbing existing samples and weight the new dataset samples according to their proximity to the sample of interest.
4. Train a weighted, interpretable model on this new dataset.
5. Explain the prediction by interpreting the local model.

### 2.4.3 ELI5

The name ELI5 is derived from the saying, “Explain it Like I’m 5”. ELI5 can be used to generate global explanations of a black-box model. The concept behind ELI5 is simply based on permuting the values of individual features—in turn, the values of each feature are shuffled, and model results are tabulated after each such shuffle. The worse the classification results after a given feature is shuffled, the more that the model depends on that feature [15].

### 2.4.4 Grad-CAM

The technique of Gradient-weighted Class Activation Map (Grad-CAM) is used to analyze CNNs. Grad-CAM assists in understanding which parts of an image a convolutional layer weights most to determine a given classification [27]. That is, Grad-CAM is a class-based localization technique for CNN interpretability.

Grad-CAM uses gradient information flowing into the last convolutional layer of a CNN to obtain a localization map of the important regions in the image, and thereby determines the importance of each pixel of the input image for the specified class. This resulting gradient weighted activation map can be overlaid on the original input image to visualize which parts of the input the CNN associates highly with a given output class.

### 2.4.5 SHAP and PDP Plots

SHapley Additive exPlanations (SHAP) is a popular XAI technique based on Shapley values. In 1951, Lloyd Shapley developed a technique to determine the contribution of each player in a multi-player game setting, and in 2012, he won the Nobel Prize in economics for his work. In Shapley’s approach, player contributions are determined by Shapley values, which have a number of desirable theoretical properties. More recently, Shapley values have been applied to XAI [21], with features in place of game-theoretic players.

In SHAP, we first compute a Shapley value for each sample and each feature, as discussed below in some detail. A Shapley value measures the contribution of a specified feature to the classification of a given sample. If we arrange the Shapley values into a matrix with the rows indexed by the samples and the columns indexed by the features, then the row corresponding to a sample can provide an explanation for the classification of the sample. For example, the largest value in a row corresponds to the feature that has the most influence on the classification of the corresponding sample. Similarly, explanations of the overall model can be determined by analyzing the Shapley values in the entire matrix.

Several types of graphs and plots can be generated based on Shapley values. Before discussing such graphs, we first provide more details on the computation of Shapley values.

Suppose that  $X$  represents a feature vector of length  $n$  of the form  $X = (f_1, f_2, \dots, f_n)$ , where each  $f_j$  is the value of a specific feature. Further, suppose that we have a model  $M$  that for each such  $X$  produces a real-valued result,  $M(X)$ . For example,  $M(X)$  could be the classification of  $X$  as determined by the model  $M$ , or it could be a probability generated by the model. For any subset  $S$  of the features  $\{f_1, f_2, \dots, f_n\}$ , let  $M_S$  be a model corresponding to  $M$ , but trained only on the features in the subset  $S$ . Then  $M_S(X)$  is the real-valued result obtained for sample  $X$ , under the restricted model  $M_S$ .

For a given sample  $X$ , we compute  $n$  Shapley values, with each value corresponding to one of the  $n$  features. We denote the Shapley value for sample  $X$ , corresponding to feature  $f_i$ , as  $\Phi_i(X)$ . The Shapley value is defined as

$$\Phi_i(X) = \frac{1}{n} \sum_{S_i} \left[ (M_{\{S_i \cup f_i\}}(X) - M_{S_i}(X)) / \binom{n-1}{|S_i|} \right] \quad (1)$$

where  $S_i$  denotes a subset of the  $n - 1$  features  $\{f_1, \dots, f_{i-1}, f_{i+1}, \dots, f_n\}$ , and the sum is over all such subsets (including the empty set, with  $M_{\emptyset}(X)$  defined to be 0). Note that the Shapley value computation consists of comparing the behavior of pairs of models applied to the sample  $X$ : One models of each pair includes the feature  $f_i$ , while the other omits  $f_i$ , with the other features unchanged. These pairwise computations are averaged over the number of subsets of a given size. The  $1/n$  term in (1) normalizes the result based on the number of features.



For example, suppose that we have four features with  $X = (f_1, f_2, f_3, f_4)$ , and that we are computing the Shapley value  $\Phi_3(X)$ . Then from equation (1), we have

$$\begin{aligned} \Phi_3(X) = \frac{1}{4} & \left( (M_{\{f_3\}}(X) - M_{\emptyset}(X)) \right. \\ & + (M_{\{f_1, f_3\}}(X) - M_{\{f_1\}}(X))/3 \\ & + (M_{\{f_2, f_3\}}(X) - M_{\{f_2\}}(X))/3 \\ & + (M_{\{f_3, f_4\}}(X) - M_{\{f_4\}}(X))/3 \\ & + (M_{\{f_1, f_2, f_3\}}(X) - M_{\{f_1, f_2\}}(X))/3 \\ & + (M_{\{f_1, f_3, f_4\}}(X) - M_{\{f_1, f_4\}}(X))/3 \\ & + (M_{\{f_2, f_3, f_4\}}(X) - M_{\{f_2, f_4\}}(X))/3 \\ & \left. + (M_{\{f_1, f_2, f_3, f_4\}}(X) - M_{\{f_1, f_2, f_4\}}(X)) \right) \end{aligned} \quad (2)$$

Shapley values can also be computed by considering all  $n!$  orderings of the features. In this formulation, for each permutation, we again sum the differences of pairs of a models, where one is trained on all features up to and including  $f_i$ , with the model trained on all features up to  $f_i$ , but not including  $f_i$ . We now discuss this approach in more detail.

For any permutation  $P$  of the features, let  $P_i$  be the initial part of the permutation before  $f_i$  appears. Then we can rewrite equation (1) as

$$\Phi_i(X) = \frac{1}{n!} \sum_P (M_{P_i \cup \{f_i\}}(X) - M_{P_i}(X)) \quad (3)$$

where the sum is over all  $n!$  permutations  $P$  of the  $n$  features  $\{f_1, f_2, \dots, f_n\}$ .

Using equation (3), the example in equation (2) can be written as

$$\begin{aligned} \Phi_3(X) = \frac{1}{24} & \left( (M_{\{\underline{f_1}, \underline{f_2}, \underline{f_3}, f_4\}}(X) - M_{\{\underline{f_1}, \underline{f_2}, f_3, f_4\}}(X)) \right. \\ & + (M_{\{\underline{f_1}, \underline{f_2}, \underline{f_4}, \underline{f_3}\}}(X) - M_{\{\underline{f_1}, \underline{f_2}, \underline{f_4}, f_3\}}(X)) \\ & + (M_{\{\underline{f_1}, \underline{f_3}, \underline{f_2}, f_4\}}(X) - M_{\{\underline{f_1}, \underline{f_3}, f_2, f_4\}}(X)) \\ & + (M_{\{\underline{f_1}, \underline{f_3}, \underline{f_4}, \underline{f_2}\}}(X) - M_{\{\underline{f_1}, \underline{f_3}, \underline{f_4}, f_2\}}(X)) \\ & + (M_{\{\underline{f_1}, \underline{f_4}, \underline{f_2}, \underline{f_3}\}}(X) - M_{\{\underline{f_1}, \underline{f_4}, \underline{f_2}, f_3\}}(X)) \\ & \vdots \qquad \qquad \qquad \vdots \\ & + (M_{\{\underline{f_4}, \underline{f_1}, \underline{f_3}, \underline{f_2}\}}(X) - M_{\{\underline{f_4}, \underline{f_1}, f_3, f_2\}}(X)) \\ & + (M_{\{\underline{f_4}, \underline{f_2}, \underline{f_1}, \underline{f_3}\}}(X) - M_{\{\underline{f_4}, \underline{f_2}, \underline{f_1}, f_3\}}(X)) \\ & + (M_{\{\underline{f_4}, \underline{f_2}, \underline{f_3}, \underline{f_1}\}}(X) - M_{\{\underline{f_4}, \underline{f_2}, f_3, f_1\}}(X)) \\ & + (M_{\{\underline{f_4}, \underline{f_3}, \underline{f_1}, \underline{f_2}\}}(X) - M_{\{\underline{f_4}, \underline{f_3}, f_1, f_2\}}(X)) \\ & \left. + (M_{\{\underline{f_4}, \underline{f_3}, \underline{f_2}, \underline{f_1}\}}(X) - M_{\{\underline{f_4}, \underline{f_3}, \underline{f_2}, f_1\}}(X)) \right) \end{aligned} \quad (4)$$

where, for clarity, we have listed the entirety of each permutations, with the underlined red parts representing the subscripts that appear in (2). Note that if there is no underlined part of a permutation, the model is  $M_{\emptyset}$ .

From the formula in (3)—and the example in (4)—we can clearly see how the Shapley value  $\Phi_i(X)$  measures the contribution of feature  $f_i$  to the classification of sample  $X$ . Specifically, a model is trained on a set of features that includes  $f_i$ , and the classification of  $X$  by that model is compared to that obtained using the same features, except that  $f_i$  is removed. Such comparisons are computed for all permutations, and the results are averaged. Rearranging terms, we see that the Shapley value is the difference between the expected outcome when feature  $f_i$  is included in the model, and the expected outcome when feature  $f_i$  is not included.

In many cases, training models for all permutations would be prohibitively costly, even for just one Shapley value. Sampling methods are used, and some of the properties of Shapley values can also play a role in making the problem computationally tractable.

As alluded to in the previous paragraph, Shapley values satisfy several useful and interesting properties. For our purposes the most relevant properties are the following.

- Efficiency — The sum of the Shapley values for  $X$  is equal to the value that the model trained on all features produces for  $X$ . That is,

$$M(X) = \sum_{i=1}^n \Phi_i(X)$$

- Symmetry — If  $M_{S \cup \{f_i\}}(X) = M_{S \cup \{f_j\}}(X)$  for all feature subsets  $S$  that include neither  $f_i$  nor  $f_j$ , then  $\Phi_i(X) = \Phi_j(X)$ .
- Linearity — The Shapley values are linear with respect to samples, that is,  $\alpha\Phi_i(X) = \Phi_i(\alpha X)$  and  $\Phi_i(X) + \Phi_i(Y) = \Phi_i(X + Y)$ .
- Null — The Shapley value of a null feature is 0, where a null feature, by definition, satisfies  $M_{S \cup \{f_i\}}(X) = M_S(X)$  for all  $S$  that do not include  $f_i$ .

The linear property implies that for a Random Forest, we can compute the Shapley values of each component decision tree and then combine the results to obtain the Shapley value for the overall model [27, Section 9.5]. A similar statement holds for boosting methods, and hence for both Random Forest and boosting models, computing Shapley values is computationally feasible.

Partial Dependence Plots (PDP) use Shapley values to visualize the marginal effect of a predictor variable on the predictive variable by plotting the average model outcome at different levels of the predictor variable [27]. This gives the average effect that a predictor variable has on the predictive variable. These values are plotted on a chart which provides evidence of the direction in which a variable affects the outcome.

### 3 Related Work

XAI is a very active field, although research into its application in the malware domain is more limited. In this section, we survey previous research that involves applications of XAI to malware classification and detection.

Manthena, et al. [23] consider XAI in the context of malware detection. The goal of this research is to determine how malware influences the behavior of virtual machines (VMs) in a cloud environment. Three different variants of SHAP are applied (KernelSHAP, TreeSHAP, and DeepSHAP), while the learning techniques considered are linear SVM, nonlinear SVM (with RBF kernel), Random Forest, a specific feed-forward neural network, and CNN, all of which are trained on a malware dataset. The researchers use the SHAP interpretations to implement feature reductions.

Yan, et al. [38] consider ante-hoc and post-hoc explanation in detail. They evaluate these techniques based on six metrics (accuracy, sparsity, completeness, stability, efficiency, and fidelity), and conclude that Layerwise Relevance Propagation (LRP) is the most efficient XAI technique. The authors also list open issues, including the potential tradeoff between accuracy and explainability.

Charmet, et al. [1] provide a comparative study of XAI for different cybersecurity tasks with the goal of determining which explanation methods could be efficiently used for each of the following: Improved trust (in the sense of increased transparency), improved classifier performance, and to explain errors in the models. They also show that XAI methods involving heatmaps and saliency maps can be easily compromised.

Ullah, et al. [35] conduct XAI experiments in the context of Android malware detection, based on both traditional features and greyscale image data. They consider pre-trained Bidirectional Encoder Representations from Transformers (BERT) models, which rely on transfer learning. LIME and SHAP are used to determine the effect of each feature on the overall accuracy of the model.

Liu, et al. [20] also use XAI approaches to explore learning models in the realm of malware detection. They consider LIME and SHAP, and the research primarily focuses on understanding the impact of temporal inconsistencies in the training data with respect to the performance of ML-based malware detection approaches.

Kinkead, et al. [14] consider the problem of explaining predictions of Android malware classification models. They consider CNN models, and they use the LIME for their XAI analysis. The authors claim that their work provides additional trust and confidence in their CNN model.

Severi, et al. [32] develop a model-agnostic methodology based on SHAP to examine the vulnerability of classifiers to adversarial attack. The research is based on static and dynamic analysis of diverse datasets, including Portable Executable (PE) files and Android applications. High-contributing features are selected using SHAP and attacks are conducted against a variety of learning models, including Random Forest, SVM, and a Deep Neural Network (DNN). These researchers claim that their explanation-guided attack method is more robust, as compared to alternative approaches.

Fan, et al. [4] provide guidelines to assess the quality, stability, and robustness of XAI approaches. They experiment with LIME, Anchor, Local Rule-based Explanations (LORE), SHAP, and LEMNA and consider several learning techniques

(MLP, Random Forest, SVM). They claim that in the domain of Android malware detection, inconsistencies in results from different XAI techniques makes it difficult to trust the explanations.

Warnecke, et al. [36] provide general recommendations related to the application of explanation methods for deep learning techniques in the security domain. A variety of XAI methods are considered, and the authors find that the Integrated Gradients and LRP methods are most effective, according to their specified criteria.

In Table 1, we summarize the papers mentioned in this section, as well as a few other relevant research papers. We note that these cited papers are relatively recent, with all having been published between 2016 and 2023.

Table 1: Selected previous work

Authors	Dataset	XAI techniques
Charmet, et al. [1]	—	Survey paper
Chen, et al. [2]	AndroZoo	LEMNA
Fan, et al. [4]	Multiple sources	LORE, SHAP, others
Feichtner and Gruber [5]	PlayDrone	LIME
Iadarola, et al. [11]	Android Malware Dataset	Grad-CAM
Kinkead, et al. [14]	Drebin	LIME
Liu, et al. [20]	AndroZoo	LIME, SHAP
Manthana, et al. [23]	VirusTotal	SHAP
Severi, et al. [32]	Grad-CAM	SHAP
Ullah, et al. [35]	CICMalDroid 2020	LIME, SHAP
Warnecke, et al. [36]	Drebin, Genome	LRP, LIME, SHAP
Wu, et al. [37]	Drebin+	XMAL
Yan, et al. [38]	—	Survey paper
Yang, et al. [40]	Drebin	Distance-based

Amongst the XAI techniques considered in this paper, SHAP appears to be the most widely studied by the research community, followed by CAM and LIME. The graph in Figure 2 charts the appearance of these three XAI technique in research papers over recent years [28].

We note in passing that the number of relevant studies focusing on evaluating XAI in the malware domain is relatively small. Further, there is currently no accepted standard method or criteria for selecting or evaluating XAI methods for malware-related problems, and hence a general recommendation as to which XAI method or methods will work well in the Android malware domain is unavailable. Thus, more research is needed in this area to determine the practical utility of XAI techniques for real-world Android malware problems.

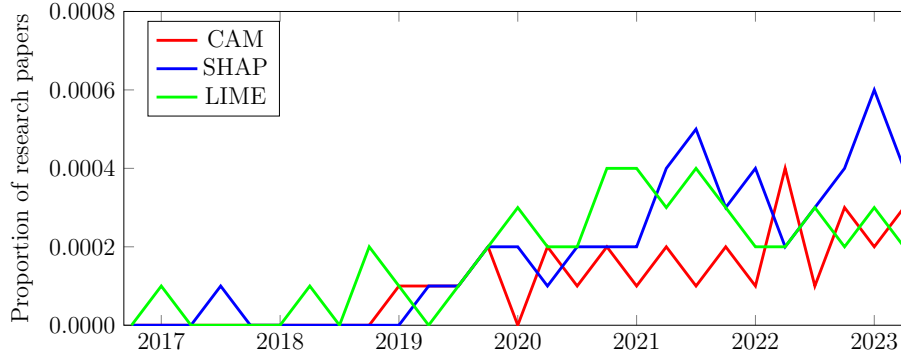


Figure 2: XAI research papers

## 4 Experiments and Results

In this section, we consider a range of XAI experiments. But first, we discuss our dataset and implementation.

### 4.1 Dataset and Implementation

We use the KronoDroid dataset [8] for all of the experiments reported in this paper. This dataset includes labeled data from 240 malware families, with 78,137 total samples, of which 41,382 are malware and 36,755 are benign Android apps. For each sample, 289 dynamic features (based on system calls) and 200 static features (e.g., `permissions`) are provided. Each malware family contains a number of samples collected over an extended period of time. Samples belonging to a malware family generally have similar characteristics and share a common code base.

To ensure a significant number of samples per family, we restrict our attention to the top 10 malware families in the KronoDroid dataset. These top 10 malware families have a total of 31,046 samples, with the percentage of samples per family illustrated in the pie graph in Figure 3.

All classic machine algorithms experiments are performed on a single host machine, while deep learning experiments are performed using the GPU on this same machine. All experiments in this research have been executed on the computer specified in Table 2.

We cleaned the data to remove irrelevant features. The cleaned dataset contains 468 features per sample. All features are standardized using a standard scaler.

In our experiments, we use accuracy and F1-score to measure the performance of each classifier. Accuracy is defined as the total number of correct predictions over the number of samples tested. The F1-score is a weighted average

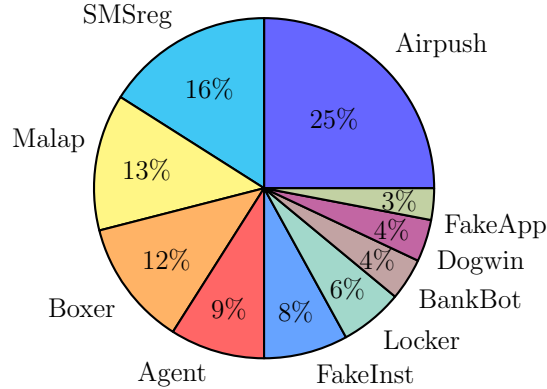


Figure 3: Top 10 malware families

Table 2: Computing resources used in experiments

Computing resource	Details
Computer	Dell XPS 13
Processor	Intel Core i5-7200U CPU @ 2.50 Ghz, 2.70 Ghz
RAM	8.0 GB
Operating System	Windows 10 Enterprise 64-bit

of precision and recall, and it is computed as

$$F1 = 2 \times \frac{(\text{Precision} \times \text{Recall})}{(\text{Precision} + \text{Recall})}$$

where

$$\text{Precision} = \frac{\text{True Positives}}{(\text{True Positives} + \text{False Positives})}$$

and

$$\text{Recall} = \frac{\text{True Positives}}{(\text{True Positives} + \text{False Negatives})}$$

As with accuracy, F1 scores fall between 0 and 1, with 1 being the best possible.

As discussed above, the primary goal of this research is to explore the utility of XAI techniques in the Android malware domain. Towards this end, we generate explanations and obtain interpretations for SVM (both linear and non-linear), Random Forest,  $k$ -NN, MLP, and CNN. We consider a wide range of XAI experiments, from generating ante-hoc explanations based a model’s inherent interpretability to post-hoc explanations. We generate post-hoc explanations using LIME, SHAP, ELI5, and PDP Plots. For CNNs, we use the model-specific technique of CAM. The package `scikit-learn` has been employed for most of the experiments, with the exception being that the `Tensorflow` and `Keras` libraries are utilized for CNNs. In all cases, we perform stratified 5-fold cross-validation.

A summary of the main hyperparameters for our various models follows.

- **SVM** — We perform preliminary tests to determine the best kernel for our nonlinear SVM, with the result being the Gaussian radial basis function (RBF).
- **Random Forest** — Based on small-scale experiments, we found that using `n_estimator = 100` and otherwise using the hyperparameter defaults in scikit-learn yielded the best results.
- **$k$ -NN** — Again, based on small-scale experiments, we selected  $k = 5$  for all  $k$ -NN experiments reported in this paper.
- **MLP** — We use a deep architecture with 300 hidden layers, rectified linear unit (ReLU) activation functions, and a learning rate of  $\alpha = 0.0001$ .
- **CNN** — We use max pooling for our CNN model. We experimented with various hyperparameters and found that an initial number of convolution filters set to 32, a filter size  $2 \times 2$ , and a dropout rate of 0.25 yielded the best results.

## 4.2 Performance of Learning Models

For the experiments in this section, we use an 80:20 stratified training:testing split. As mentioned above, all models are trained using only the top 10 malware families in the KronoDroid dataset. The results of our experiments are shown in Table 3. We observe that Random Forest performs best, while MLP is second best. In addition, all models perform reasonably well, with the accuracy of the worst-performing model being within 4% of that of Random Forest.

Table 3: Performance of ML and DL models

Model	Accuracy	Precision	Recall	F1
Linear SVM	0.9180	0.9194	0.8719	0.8917
RBF-SVM	0.8917	0.8937	0.8917	0.8898
Random Forest	0.9322	0.9318	0.9322	0.9314
$k$ -NN	0.9061	0.9052	0.9061	0.9054
MLP	0.9209	0.9206	0.9209	0.9207
CNN	0.9076	0.9089	0.8976	0.9091

## 4.3 XAI Results

In this section, we apply the explainability techniques in Section 2.4 to our models, and we discuss the results. Note that three versions of SHAP are considered here: For SVM models we use KernelSHAP, for Random Forest we use TreeSHAP, and for MLP we use DeepSHAP.

### 4.3.1 Linear SVM and Random Forest Feature Importance

We calculate feature importance by extracting the feature weights from the linear SVM and Random Forrest models. Figures 4 and 5 show the top 10 most important features for our linear SVM and Random Forrest models, respectively. We observe that `BLIND_DEVICE_ADMIN`, `SET_WALLPAPER`, and `READ_SMS` are the main drivers of model predictions for the linear SVM, while for Random Forrest, `ACCESS_COARSE_LOCATION`, `total_perm`, and `read` contribute the most. We find that the feature importance results on the train and test sets are consistent for both models, which indicates that they are not overfitting on the KronoDroid dataset. Extracting such feature coefficients is not possible for a nonlinear SVM kernel.

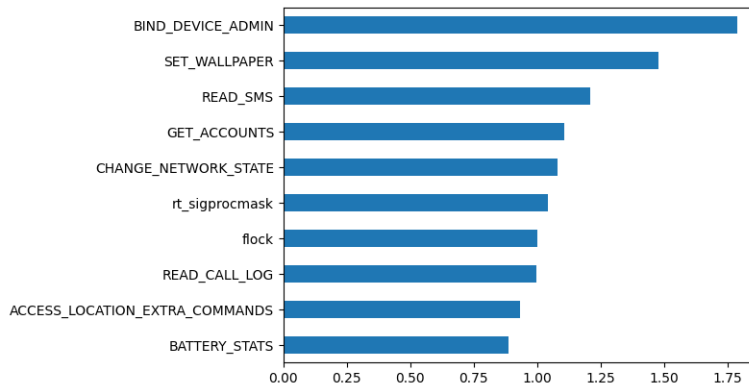


Figure 4: Feature importance from linear SVM

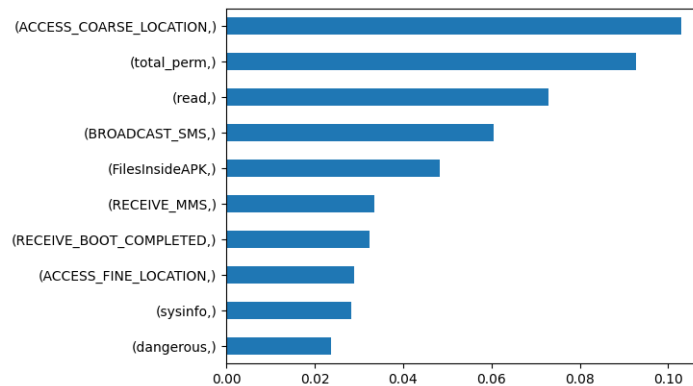


Figure 5: Feature importance from Random Forest

### 4.3.2 ELI5 Feature Importance

Recall that ELI5 is a permutation-based technique that measures the change in model error after the values of a single feature have been shuffled. We use the



ELI5 library in Python to calculate permutation importance [16].

Table 4 shows the permutation importance for our Random Forest model. The values at the top of the ELI5 output are the most important features in our model, while those at the bottom matter the least. The first number in each row indicates how much the model performance decreased with random shuffling, using the same performance metric as the original model—in this case, we use mean squared error (MSE). The number after the  $\pm$  measures how performance varied over the reshuffling, in terms of the range of values. For example, shuffling the data of the `SEND_SMS` feature caused the Random Forest MSE to vary by 0.0010. By this measure, the top three features are `SEND_SMS`, `RECEIVE_BOOT_COMPLETED`, and `TimesSubmitted`.

Table 4: ELI5 feature importance for Random Forest

Weight	Feature
0.0033 $\pm$ 0.0010	<code>SEND_SMS</code>
0.0032 $\pm$ 0.0003	<code>RECEIVE_BOOT_COMPLETED</code>
0.0021 $\pm$ 0.0020	<code>TimesSubmitted</code>
0.0015 $\pm$ 0.0011	<code>GET_ACCOUNTS</code>
0.0014 $\pm$ 0.0016	<code>FilesInsideAPK</code>
0.0012 $\pm$ 0.0006	<code>GET_TASKS</code>
0.0011 $\pm$ 0.0017	<code>UFileSize</code>
0.0011 $\pm$ 0.0005	<code>READ_EXTERNAL_STORAGE</code>
0.0010 $\pm$ 0.0002	<code>READ_PHONE_STATE</code>
0.0008 $\pm$ 0.0006	<code>dangerous</code>
0.0008 $\pm$ 0.0013	<code>signature</code>
0.0008 $\pm$ 0.0002	<code>SYSTEM_ALERT_WINDOW</code>
0.0007 $\pm$ 0.0011	<code>mprotect</code>
0.0006 $\pm$ 0.0005	<code>WRITE_SECURE_SETTINGS</code>
0.0005 $\pm$ 0.0009	<code>sysinfo</code>
0.0005 $\pm$ 0.0004	<code>CHANGE_CONFIGURATIONS</code>
0.0005 $\pm$ 0.0009	<code>fsync</code>
0.0005 $\pm$ 0.0012	<code>prctl</code>
0.0004 $\pm$ 0.0004	<code>READ_LOGS</code>
0.0004 $\pm$ 0.0008	<code>fchmod</code>
$\vdots$	$\vdots$
(448 more)	(448 more)

We note that only four of the top 10 features listed in the bar graph in Figure 5 appear among the top 20 features in Table 4. This points to the issue of inconsistency between XAI analysis techniques.

### 4.3.3 LIME Interpretations

LIME provides a list of the importance of each feature in model prediction relative to a specified sample. Recall that LIME relies on a simplified local model for feature ranking.

KronoDroid dataset consists of tabular data, so we define a tabular explainer object in LIME. The trained model, features used in training, and labels of target classes serve as inputs, and the results are based on the test data.

Figures A.1(a) through (d) in the appendix show the LIME explanations for the RBF-SVM,  $k$ -NN, Random Forest, and MLP models, respectively, based on the first sample of the test dataset for each model. All models correctly classify this first sample of test data with high confidence as Locker ransomware. The left side of the LIME explanation shows the probability with which the sample is classified as ransomware—the pink color indicates that the contribution is towards the ransomware family, while the purple color indicates that the contribution is towards Malap family. We observe that these figures show that the RBF-SVM,  $k$ -NN, Random Forest, and MLP models classify this specific sample as ransomware with probabilities of 0.82, 1.0, 1.0, and 1.0, respectively.

The LIME output in Figure A.1(a) shows the classification result for the top two highest probability classes for this specific sample. In the middle of the figure, there is a list of rules that gives the reason why this sample belongs to the class ransomware, and it identifies and lists the features that contribute most to the prediction, in order of importance. On the right side of the figure, there is a table—pink values are the reason for the final prediction, while green values are the reasons that do not support the prediction outcome. In this case, `SEND_SMS` points strongly towards a ransomware classification, while there are four features that are against the ransomware classification, but only weakly so.

Figures A.2(a) through (d) in the appendix show the LIME explanations for RBF-SVM,  $k$ -NN, Random Forest, and MLP models, respectively, for a sample in the Malap family that is misclassified as BankBot by all of these models. The (mis)classification probabilities are 0.93, 0.79, 0.57, and 1.0 for the RBF-SVM,  $k$ -NN, Random Forest, and MLP models, respectively. In the figures, orange values are the reason for the final prediction, and green color values are those that do not support the predicted outcome. Figure A.2(a), for example, shows that the feature `SEND_SMS` contributes to a Bankbot and a ransomware classifications, both of which are incorrect, but since there are fewer negative factors for Bankbot, it is the selected classification. Interestingly, Random Forest is the only model that gives any significant weight to the possibility of this sample being in the (correct) Malap family, but only with a probability of 0.17.

We observe that the LIME interpretations for the RBF-SVM and MLP models are the most similar pair in Figure A.1 and, arguably, also in Figure A.2. This is not surprising, as nonlinear SVMs and MLPs are closely related models, in the sense that an MLP can be viewed as an SVM-like model, where the equivalent of the kernel function is learned [34]. Based on the LIME interpretations in these figures, Random Forest appears to be the most different from the other three models. It is somewhat surprising that the  $k$ -NN and Random Forest results are not more similar, as those techniques are both neighborhood-based techniques [34].

### 4.3.4 Grad-CAM Interpretation

For this experiment, we represent the input array as an image. To generate the images, we first order the 468 features from highest to lowest importance, as determined by the Random Forest model. For each sample, we put these ordered feature values into a  $22 \times 22$  array (with 0 padding for the final 16 elements), which we then interpret as a grayscale image for our CNN model.

We use `iNNvestigate` library to generate Grad-CAM output on our CNN model output. The method `create_analyzer` of `iNNvestigate` determines the components of the input that correspond to the output. It then determines the importance of an input pixel based on how much a change in the pixel affects the output.

We analyze an image from the test dataset with the `gradient` function, which gives the gradient of the output neuron with respect to the input. Figure 6(a) shows the sample test image reshaped as  $22 \times 22$  grayscale image as discussed above. Figure 6(b) shows the Grad-CAM output for the prediction made by the CNN model for this sample. We can visually verify which pixels (equivalently, features) in the input image the CNN is emphasizing when making its classification. For example, the Grad-CAM image shows a dark red pixel in row 1, column 12, indicating that the corresponding feature is one of the most important to the CNN classification of this particular sample.

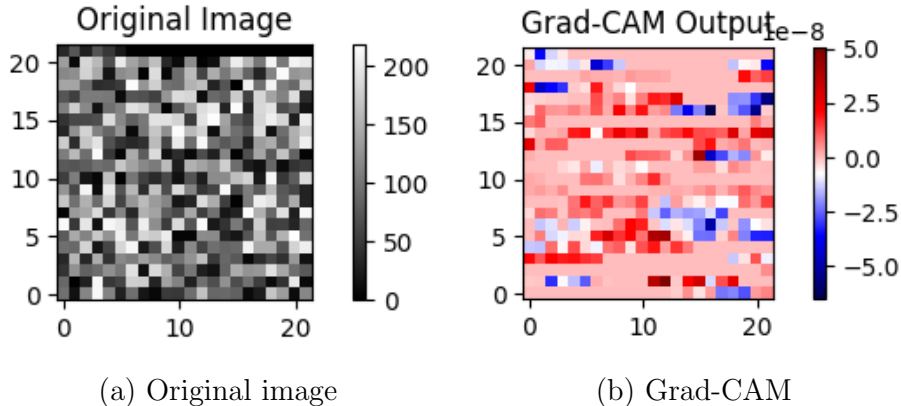


Figure 6: Grad-CAM example

We observe that the feature importance determined by Grad-CAM is much different from that of the Random Forest model. This follows, since the features in the original image are ordered from highest to lowest importance, according to the Random Forest model weights, yet there is only a slight bias towards more important features in the lower region of the Grad-CAM image. We conclude that the Random Forest and CNN models appear to be using much different criteria to make their classification decisions.

### 4.3.5 SHAP Interpretations and PDPs

We use `KernelSHAP` to generate explanations for our SVM and  $k$ -NN models, `DeepSHAP` for our MLP, and `TreeSHAP` for the Random Forest model. It is well-known that `KernelSHAP` and `DeepSHAP` are much more costly to compute, as compared to `TreeSHAP` [39].

Due to the high computational cost we use Recursive Feature Elimination (RFE) based on Random Forest models to determine which features to sample. The graph in Figure 7 shows that the accuracy of the Random Forest model does not improve, provided that at least the top 10 features are selected. Hence, we select these top 10 features to sample for each of the models under consideration.

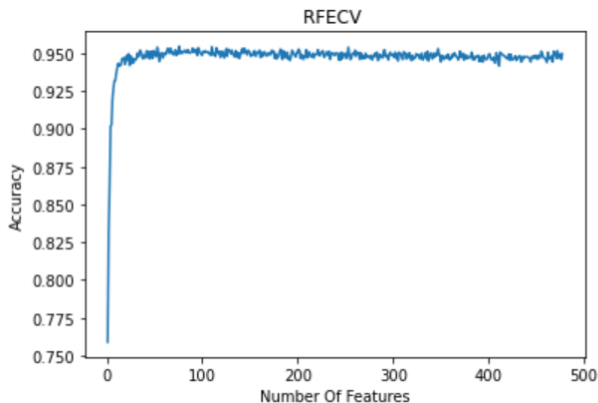


Figure 7: Random Forest RFE accuracy

For our experiments, `TreeSHAP` only required about 53 seconds to complete execution on a dataset of size 41,382, while `KernelSHAP` required about 1 hour for a comparable experiment. We found that `DeepSHAP` was comparable in runtime to `KernelSHAP`. For comparison, for the LIME experiments discussed in Section 4.3.3, the execution time was on the order of 30 seconds.

Using global model interpretation techniques, we can see how our model behaves in general. Toward this end, we generate two SHAP global model interpretation plots, specifically, a SHAP variable importance plot and a SHAP dependence plot.

We use `shap.summary_plot` function with `plot_type` set to `bar` to generate the variable importance plots. Figures 8(a) through (d) provide these SHAP global explanations for the RBF-SVM, Random Forest,  $k$ -NN, and MLP models, respectively. In these plots, the  $x$ -axis denotes the average impact on the model output (i.e., the mean SHAP value across all relevant samples) of the specified variable. It is interesting to note that the top two ranking features for all of the models are `dangerous` and `total_perm`. These graphs enable us to easily compare the relative contribution of the listed features for each model.

The SHAP values appear in the form of a beeswarm plot in Figure 9. The function `shap.summary_plot` was used to produce this plot. Here, the  $x$ -axis

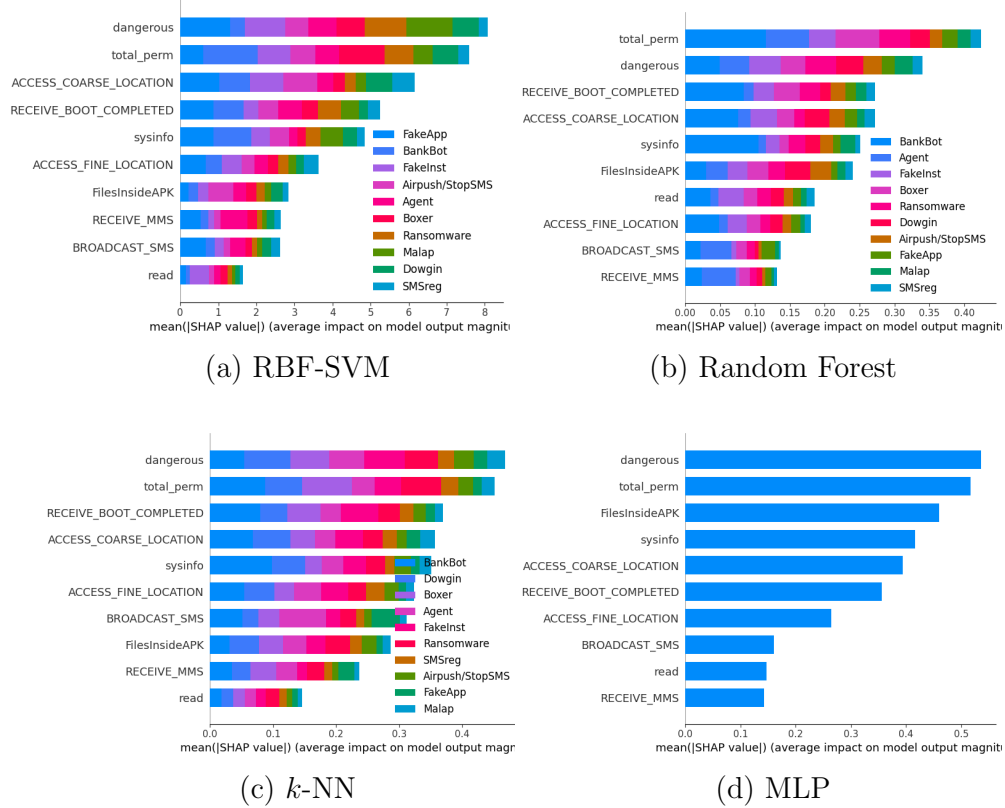


Figure 8: Variable importance plots

indicates the Shapley value, while the  $y$ -axis lists the 10 features under consideration. Shapley values corresponding to a given feature are plotted for all samples in the test set, with the thickness of the “swarm” representing the density of points. The color-coding represents the raw value of the feature, with blue indicating a low value and red corresponding to a high value. Thus, we obtain insight into the relationship of raw features and their predictive strength via the Shapley values.

From Figure 9, we make the following observations.

1. The plot lists the features in descending order of importance which, of course, matches the results in Figure 8(d).
2. For most of the features, raw values that are low are more predictive than high values, with this being especially clear for the `sysinfo` and `FilesInsideAPK` features.
3. Curiously, the two highest ranked features behave somewhat differently than the other features. Specifically, the raw high-low values of the feature `total_perm` appears to have little correlation to the corresponding Shapley values and, to a somewhat lesser extent, this also appears to be the case for the `dangerous` feature.

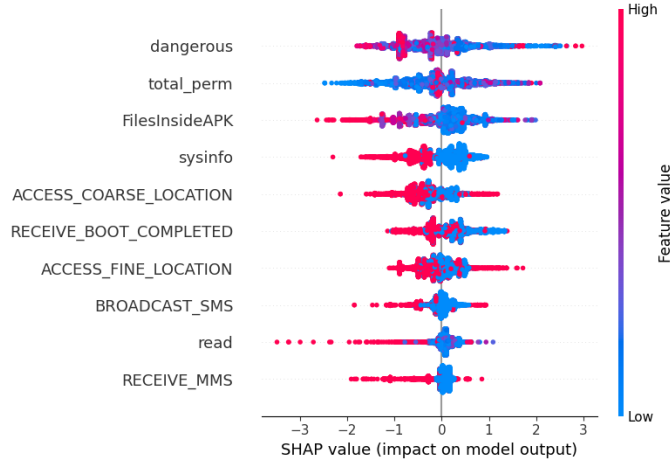


Figure 9: MLP global interpretation value plot

Partial Dependence Plots (PDP) show the average manner in which machine-learned response functions changes, based on the values of two input variables of interest, while averaging out the effects of all other input variables. PDP plots enhance our understanding of a model by showing interactions between variables and dependent variables in complex models. PDP plots can also enhance trust, provided that observed relationships conform to domain knowledge expectations.

We generate PDP plots using the `dependence_plot` method. This function automatically includes as the second variable the feature that interacts most strongly with the selected variable. PDP plots with the `dangerous` feature selected are shown in Figures 10(a) through (d) for our RBF-SVM,  $k$ -NN, Random Forest, and MLP models, respectively. We note that the `dangerous` feature is discrete, with values in the set  $\{0, 1, 2, \dots, 25\}$ .

We observe that for the RBF-SVM model in Figure 10(a) there is an approximately linear relationship between the raw value of `dangerous` in the range from 0 to 13 and the corresponding Shapley values. Furthermore, over the range of 2 to 13, higher `dangerous` values are associated with a progressively higher proportion of high values for `ACCESS_COARSE_LOCATION`, and beyond 13, only high values of `ACCESS_COARSE_LOCATION` occur.

Figures 11(a) through (d) show PDP plots with the feature `total_perm` selected for our RBF-SVM,  $k$ -NN, Random Forest, and MLP models, respectively. We observe that the RBF-SVM model in Figure 11(a) shows a linear relationship between the raw value of the `total_perm` and the Shapley values. Also, below a `total_perm` value of about 10, the corresponding `dangerous` values are low, while above that threshold, they are predominantly high.

Finally, we illustrate a local explanation for an individual sample using the SHAP `force_plot` method. This method requires the following three inputs.

1. The average of the model output over the training data, which serves as the base value used to generate the force plot.

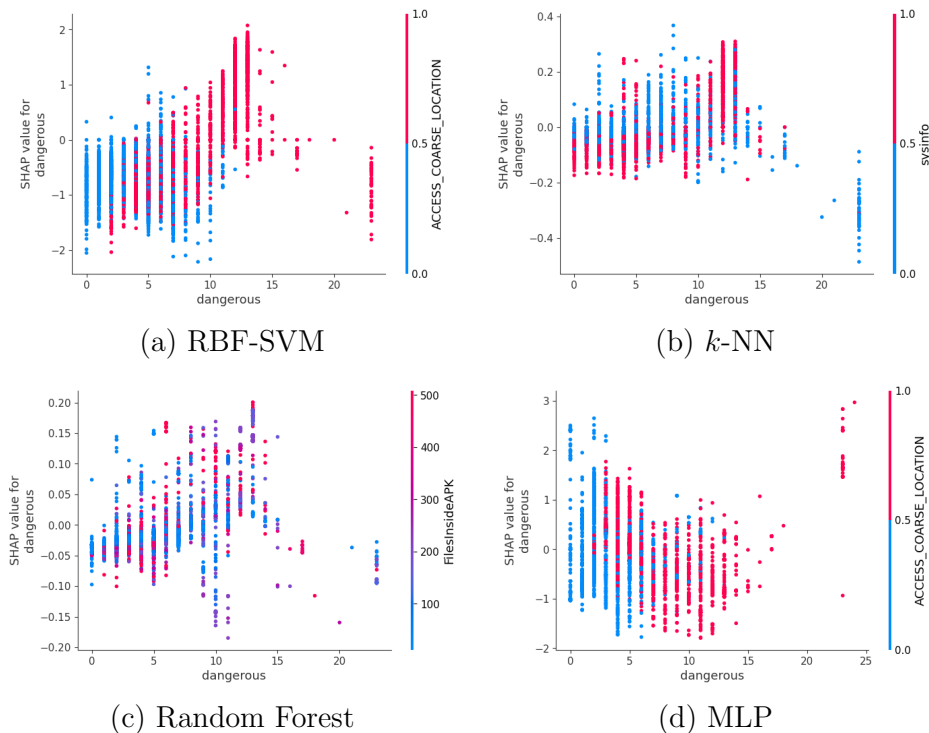


Figure 10: PDP plots (**dangerous**)

2. The Shapley values, as computed on training data.
3. The sample for which we wish to obtain a local explanation.

Figure 12 shows the SHAP force plot generated for our MLP model, based on the last sample in the test dataset. Features that push the prediction higher (to the right) are shown in red, while those pushing the prediction lower are in blue. In this case, the base value is 3.1, and based on the Shapley values, `sysinfo` and `total_perm` have highest positive impact on the classification, with `dangerous`, `ACCESS_COARSE_LOCATION`, and `FilesInsideAPK` also having positive impact. For this particular sample, no features have a significant negative impact on the classification, as indicated by the lack of any “force” in the blue direction.

In summary, Shapley values indicate how much a feature contributes to the prediction of a given sample, and this contribution can be positive or negative. If a feature is positively correlated to the target at a value higher than the average, it will contribute positively to the prediction. On the other hand, if a feature is negatively correlated to the target, it will contribute negatively to the prediction. Furthermore, a wealth of information can be gleaned from Shapley values using a number of different plotting strategies.

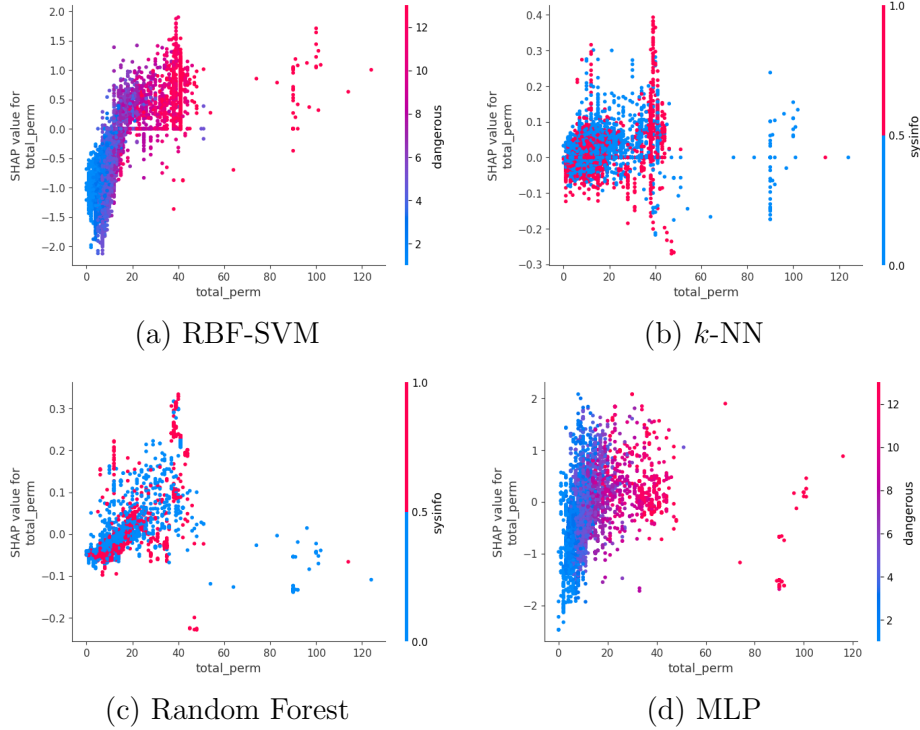


Figure 11: PDP plots (`total_perm`)

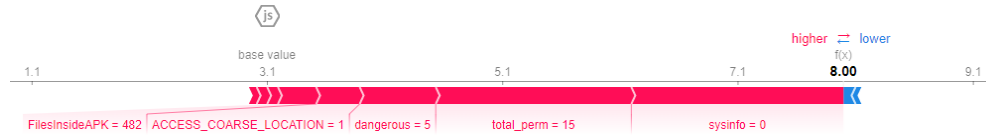


Figure 12: SHAP explanations for MLP (last observation)

## 5 Conclusion and Future Work

In this paper, we provided a selective survey of previous work involving the application of XAI techniques to detection and classification problems in the malware domain. We then performed a comparative study of several XAI techniques for a variety of models, including classic ML models (linear SVM, RBF-SVM, Random Forest, and  $k$ -NN) and deep learning models (MLP and CNN). When trained on a challenging Android malware multiclass problem, we found that Random Forest performed best among these models, followed closely by MLP, with all of the models performing within a few percentage points of the best model.

We applied a several well-known XAI techniques (ELI5, LIME, CAM, and SHAP) to our trained models. All of these XAI techniques provided interesting information about the learning models to which they were applicable. Although relatively costly to compute, SHAP explanations were particularly informative.



ELI5 proved effective at providing global explanations, while LIME generated explanations at a granular level of individual samples. CAM uncovered details of the inner workings of our CNN model, which otherwise would have remained very opaque. SHAP provided many insights, including PDP plots that enabled us to visualize relationships between pairs of features.

There are many potential avenues for future research. It would certainly be useful to have guidelines for determining which XAI techniques are most likely to produce useful results for problems in the malware domain. Of course, it would also be useful to have such guidelines more generally, that is, for a given model type when trained on a dataset from a specific problem domain. Additional work to quantify XAI results is another important fundamental research topic.

Finally, we note that the work in [4] purports to show that "... explanation results obtained in the malware analysis domain cannot achieve a consensus in general ...". Some of our results presented in Section 4 do raise questions of consistency. This issue of consistency (or lack thereof) is perhaps the most pressing concern in the entire field of XAI, and hence further research on this topic is needed.

## References

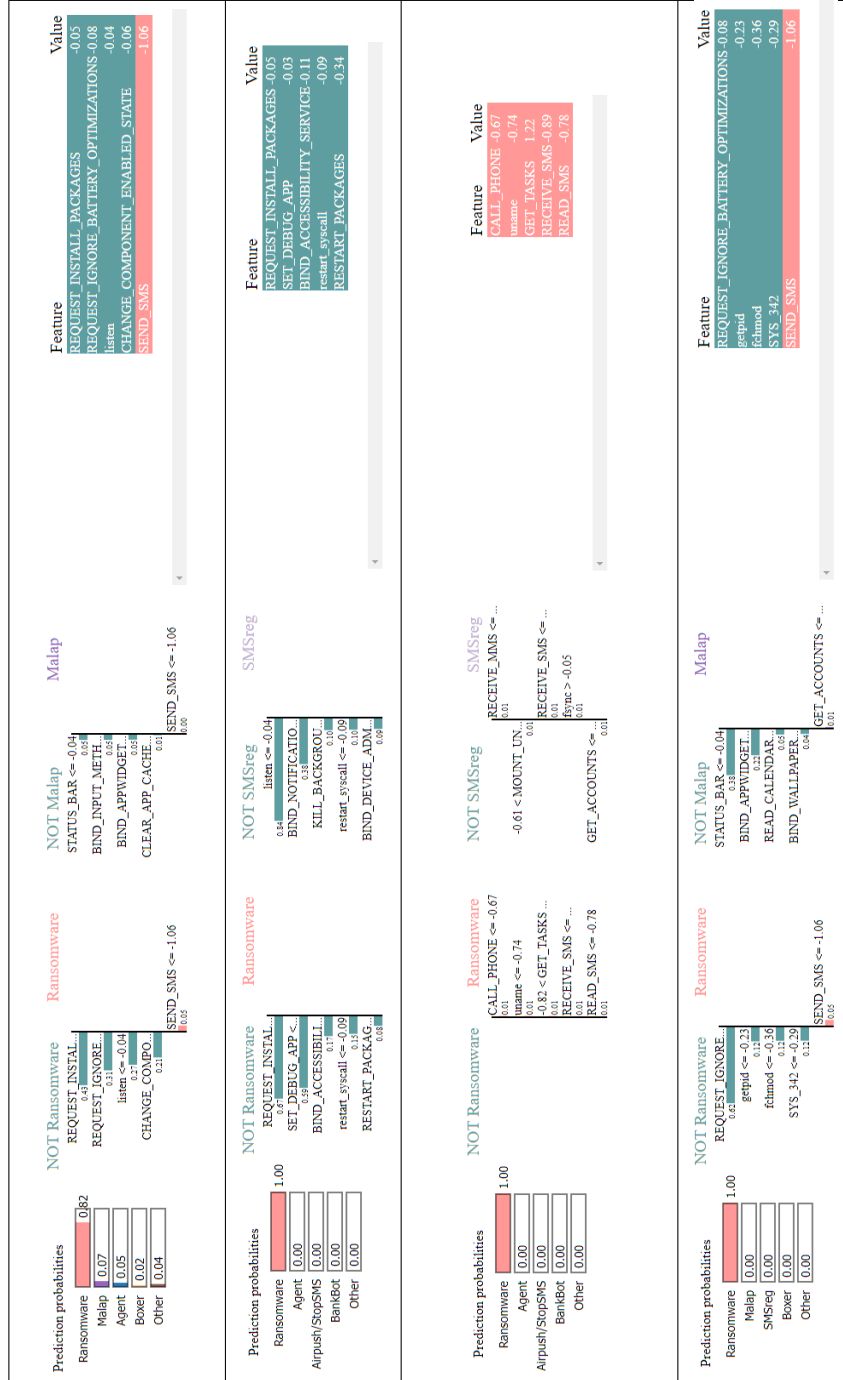
- [1] Fabien Charmet, Harry Tanuwidjaja, Solayman Ayoubi, Pierre-Francois Gimenez, Yufei Han, Houda Jmila, Gregory Blanc, Takeshi Takahashi, and Zonghua Zhang. Explainable artificial intelligence for cybersecurity: A literature survey. *Annals of Telecommunications*, 77, 2022.
- [2] Simin Chen, Soroush Bateni, Sampath Grandhi, Xiaodi Li, Cong Liu, and Wei Yang. DENAS: Automated rule generation by knowledge extraction from neural networks. In *Proceedings of ESEC/FSE 2020*, pages 813–825, 2020.
- [3] Anusha Damodaran, Fabio Di Troia, Corrado Aaron Visaggio, Thomas H. Austin, and Mark Stamp. A comparison of static, dynamic, and hybrid analysis for malware detection. *Journal of Computer Virology and Hacking Techniques*, 13(1):1–12, 2017.
- [4] Ming Fan, Wenying Wei, Xiaofei Xie, Yang Liu, Xiaohong Guan, and Ting Liu. Can we trust your explanations? sanity checks for interpreters in Android malware analysis. <https://arxiv.org/abs/2008.05895>.
- [5] Johannes Feichtner and Stefan Gruber. Understanding privacy awareness in Android app descriptions using deep learning. In *Proceedings of the Tenth ACM Conference on Data and Application Security and Privacy*, pages 203–214, 2020.
- [6] G DATA blog: Cyber attacks on Android devices on the rise. <https://www.gdatasoftware.com/blog/2018/11/31255-cyber-attacks-on-android-devices-on-the-rise>, 2018.

- [7] Google. AI explanations whitepaper. <https://storage.googleapis.com/cloud-ai-whitepapers/AI%20Explainability%20Whitepaper.pdf>.
- [8] Alejandro Guerra-Manzanares, Hayretin Bahsi, and Sven Nömm. KronoDroid: Time-based hybrid-featured dataset for effective Android malware detection and characterization. *Computers & Security*, 110(C):8–14, 2021.
- [9] David Gunning, Mark Stefik, Jaesik Choi, Timothy Miller, Simone Stumpf, and Guang-Zhong Yang. XAI: Explainable artificial intelligence. *Science Robotics*, 4(37), 2019.
- [10] Patrick Hall and Navdeep Gill. *An Introduction to Machine Learning Interpretability*. O’Reilly Media and H2O, second edition, 2019.
- [11] Giacomo Iadarola, Fabio Martinelli, Francesco Mercaldo, and Antonella Santone. Towards an interpretable deep learning model for mobile malware detection and family identification. *Computers & Security*, 105:102–198, 2021.
- [12] IBM. What is random forest? <https://www.ibm.com/topics/random-forest>.
- [13] Kaspersky. Zeus virus. <https://www.kaspersky.com/resource-center/threats/zeus-virus>, 2023.
- [14] Martin Kinkead, Stuart Millar, Niall McLaughlin, and Philip O’Kane. Towards explainable CNNs for Android malware detection. *Procedia Computer Science*, 184:959–965, 2021.
- [15] Mikhail Korobov and Konstantin Lopuhin. ELI5. <https://eli5.readthedocs.io/en/latest/index.html>, 2016.
- [16] Mikhail Korobov and Konstantin Lopuhin. ELI5: Permutation importance. [https://eli5.readthedocs.io/en/latest/blackbox/permutation\\_importance.html](https://eli5.readthedocs.io/en/latest/blackbox/permutation_importance.html), 2016.
- [17] LIME. <https://github.com/marcotcr/lime>.
- [18] Pantelis Linardatos, Vasilis Papastefanopoulos, and Sotiris Kotsiantis. Explainable AI: A review of machine learning interpretability methods. *Entropy*, 23(1), 2021.
- [19] Yue Liu, Chakkrit Tantithamthavorn, Li Li, and Yepang Liu. Deep learning for Android malware defenses: A systematic literature review. *ACM Computing Surveys*, 55(8):1–36, 2022.
- [20] Yue Liu, Chakkrit Tantithamthavorn, Li Li, and Yepang Liu. Explainable AI for Android malware detection: Towards understanding why the models perform so well? <https://arxiv.org/abs/2209.00812>, 2022.
- [21] Scott Lundberg and Su-In Lee. A unified approach to interpreting model predictions. *Advances in Neural Information Processing Systems*, 30:4765–4774, 2017. <http://arxiv.org/abs/1705.07874>.

- [22] Malware categories. <https://developers.google.com/android/play-protect/phacategories>, 2023.
- [23] Harikha Manthena, Jeffrey C. Kimmel, Mahmoud Abdelsalam, and Maanak Gupta. Analyzing and explaining black-box models for online malware detection. *IEEE Access*, 11:25237–25252, 2023.
- [24] MathWorks. What is interpretability? <https://it.mathworks.com/discovery/interpretability.html>.
- [25] Microsoft Blog. Win32/winwebsec. <https://www.microsoft.com/en-us/wdsi/threats/malware-encyclopedia-description?Name=Win32/Winwebsec>, 2017.
- [26] Pradeepta Mishra. *Model Explainability and Interpretability*. Apress Publishers, 2022.
- [27] Christoph Molnar. *Interpretable Machine Learning*. Independently published, second edition, 2022. <https://christophm.github.io/interpretable-ml-book>.
- [28] PapersWithCode: Class-activation map. <https://paperswithcode.com/method/cam>.
- [29] Saeid Rezaei, Ali Afraz, Fereidoon Rezaei, and Mohammad Reza Shamani. Malware detection using opcodes statistical features. In *8th International Symposium on Telecommunications*, IST, pages 151–155, 2016.
- [30] Denis Rothman. Exploring LIME explanations and the mathematics behind it. <https://www.codemotion.com/magazine/ai-ml/lime-explainable-ai/>, 2020.
- [31] scikit-learn. <https://scikit-learn.org/stable/modules/generated/sklearn.svm.SVC.html>.
- [32] Giorgio Severi, Jim Meyer, Scott Coull, and Alina Oprea. Explanation-guided backdoor poisoning attacks against malware classifiers. In *30th USENIX Security Symposium*, USENIX Security 21, pages 1487–1504, 2021.
- [33] Mark Stamp. *Information Security: Principles and Practice*. Wiley, third edition, 2021.
- [34] Mark Stamp. *Introduction to Machine Learning with Applications in Information Security*. Chapman and Hall/CRC Press, second edition, 2023.
- [35] Farhan Ullah, Amjad Alsirhani, Mohammed Mujib Alshahrani, Abdullah Alomari, Hamad Naeem, and Syed Aziz Shah. Explainable malware detection system using transformers-based transfer learning and multi-model visual representation. *Sensors*, 22(18), 2022.
- [36] Alexander Warnecke, Daniel Arp, Christian Wressnegger, and Konrad Rieck. Evaluating explanation methods for deep learning in security. <https://arxiv.org/abs/1906.02108>, 2020.

- [37] Bozhi Wu, Sen Chen, Cuiyun Gao, Lingling Fan, Yang Liu, Weiping Wen, and Michael R. Lyu. Why an Android app is classified as malware? towards malware classification interpretation. <https://arxiv.org/abs/2004.11516>, 2020.
- [38] Feixue Yan, Sheng Wen, Surya Nepal, Cecile Paris, and Yang Xiang. Explainable machine learning in cybersecurity: A survey. *International Journal of Intelligent Systems*, 37(12):12305–12334, 2022.
- [39] Jilei Yang. Fast TreeSHAP: Accelerating SHAP value computation for trees. <https://arxiv.org/abs/2109.09847v3>, 2021.
- [40] Limin Yang, Wenbo Guo, Qingying Hao, Arridhana Ciptadi, Ali Ahmadzadeh, Xinyu Xing, and Gang Wang. CADE: Detecting and explaining concept drift samples for security applications. In *30th USENIX Security Symposium*, USENIX Security 21, pages 2327–2344, 2021.

# Appendix



(a) RBF-SVM (b)  $k$ -NN (c) Random Forest (d) MLP  
 Figure A.1: LIME explanations for correctly classified sample



(a) RBF-SVM (b) k-NN (c) Random Forest (d) MLP  
 Figure A.2: LIME explanations for incorrectly classified sample